Shortcomings of the Winkler Model in the Assessment of Sectioned Tunnels under Seismic Loading

Andersen, Lars; Lyngs, Jakob Hausgaard

Publication date:
2009

Document Version
Publisher's PDF, also known as Version of record

Shortcomings of the Winkler model in the assessment of sectioned tunnels under seismic loading

Lars Andersen & Jakob Hausgaard Lyngs

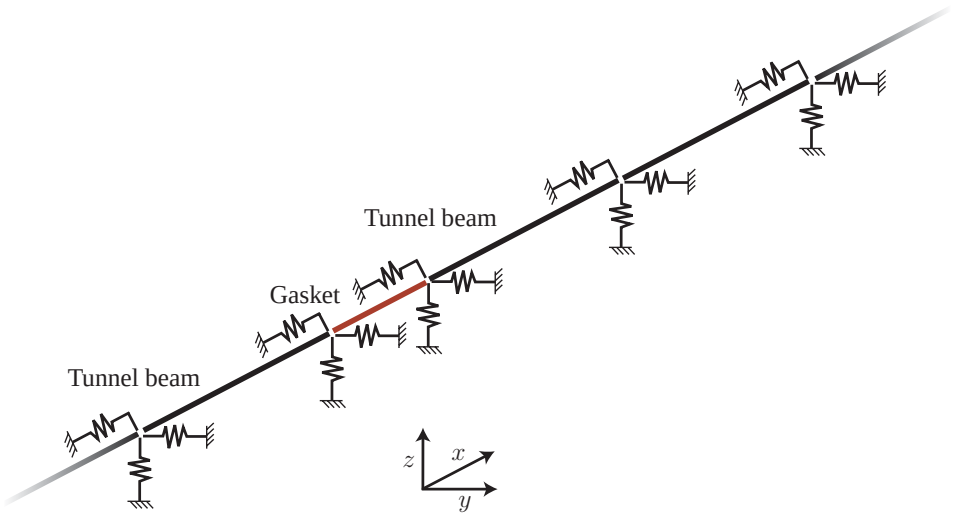

ISSN 1901-7278
DCE Technical Memorandum No. 10

AALBORG UNIVERSITY
Department of Civil Engineering

Aalborg University
Department of Civil Engineering
Structural Mechanics

DCE Technical Memorandum No. 10

Shortcomings of the Winkler model in the assessment of sectioned tunnels under seismic loading

by

Lars Andersen & Jakob Hausgaard Lyngs

May 2009

Scientific Publications at the Department of Civil Engineering

Technical Reports are published for timely dissemination of research results and scientific work carried out at the Department of Civil Engineering (DCE) at Aalborg University. This medium allows publication of more detailed explanations and results than typically allowed in scientific journals.

Technical Memoranda are produced to enable the preliminary dissemination of scientific work by the personnel of the DCE where such release is deemed to be appropriate. Documents of this kind may be incomplete or temporary versions of papers—or part of continuing work. This should be kept in mind when references are given to publications of this kind.

Contract Reports are produced to report scientific work carried out under contract. Publications of this kind contain confidential matter and are reserved for the sponsors and the DCE. Therefore, Contract Reports are generally not available for public circulation.

Lecture Notes contain material produced by the lecturers at the DCE for educational purposes. This may be scientific notes, lecture books, example problems or manuals for laboratory work, or computer programs developed at the DCE.

Theses are monograms or collections of papers published to report the scientific work carried out at the DCE to obtain a degree as either PhD or Doctor of Technology. The thesis is publicly available after the defence of the degree.

Latest News is published to enable rapid communication of information about scientific work carried out at the DCE. This includes the status of research projects, developments in the laboratories, information about collaborative work and recent research results.

Published 2009 by
Aalborg University
Department of Civil Engineering
Sohngaardsholmsvej 57,
DK-9000 Aalborg, Denmark

Printed in Denmark at Aalborg University

ISSN 1901-7278 DCE Technical Memorandum No. 10

Special print of paper submitted to *The Twelfth International Conference on Civil, Structural and Environmental Engineering Computing*, 1–4 September 2009, Madeira, Portugal.

Shortcomings of the Winkler model in the assessment of sectioned tunnels under seismic loading

L. Andersen[†] **and J.H. Lyngs**[‡]

[†]*Department of Civil Engineering, Aalborg University, Aalborg Denmark*
[‡]*COWI, Århus, Denmark*

Abstract

A Winkler-type model is often applied in the design of tunnels subject to seismic loading. Since the subgrade stiffness is modelled by disjoint springs, distributed continuously along the tunnel, the model does not account for retroaction via the soil. This may not be a problem in the design of tunnels with a uniform cross section. However, for sectioned tunnels divided into a number of elements, erroneous results may be expected—especially regarding the relative deformations at the joints. In this paper, the results of a Winkler model are compared with a full three-dimensional continuum finite-element solution, using a planned tunnel at Thessaloniki, Greece, as a case study. The aim of the analysis is to quantify the inaccuracy of the Winkler model in the prediction of damage at a gasket between two tunnel elements.

Keywords: Tunnel design; finite elements; earthquake; soil dynamics.

1 Introduction

In regions with high seismic activity, earthquakes are typically critical factors in the design of engineering structures. In the case of extended underground structures such as tunnels, the incoherence of the ground motion along structure must be considered. Furthermore, a computational model must account for the actual geometry and material behaviour of the tunnel and soil at a given location. Therefore, simple closed-form solutions are generally not available. Even the most advanced analytical solutions are restricted to simple geometries of tunnels, e.g. cylindrical shells with uniform cross sections [1].

To allow the analysis of complex geometries and seismic loading conditions, numerical models may be applied, e.g. the boundary-element method [2]. Full three-dimensional finite-element analysis is another possibility [1, 3], but such analyses are

time consuming regarding the preprocessing of the model as well as the computation time. Therefore, for the design of tunnels subjected to seismic loading, an alternative method is required that allows fast computations with low restriction on the geometrical and material properties as well as the nature of the earthquake. For that reason, the Winkler model has often been applied to the analysis of tunnels subject to earthquake excitation [4, 5, 6]. In spite of its simplicity it has been found to provide reasonable results. However, the Winkler model may significantly underestimate the stiffness at the joints in tunnels with a nonhomogeneous cross section, provided that some parts of the tunnel are considerably more flexible than the surrounding soil.

Hence, in the present paper the Winkler-type model in utilised to the analysis of a sectioned immersed tunnel. A case study is performed on the planned six-lane road toll tunnel to pass under Thermaikos Gulf outside the city centre of Thessaloniki, Greece. The tunnel is about 4 km long with a central part consisting of eight tunnel elements made of precast reinforced concrete and connected by Gina gaskets at the joints [7]. The Winkler model is outlined in Section 2, including a description of the bedrock motion and a model of the wave propagation through layered soil, similar to the SHAKE code [8]. Section 3 describes the three-dimensional continuum finite-element model utilised as reference. The results of the two models are compared and discussed in Section 4, and a final conclusion is given in Section 5.

2 Winkler model of the tunnel

In the Winkler model, the tunnel is treated as a beam and the soil is modelled by three independent systems of springs, attached continuously along the tunnel as illustrated in Fig. 1. The earthquake motion is applied by forced displacements at the external endpoints of the subgrade springs with no interaction between the responses in the

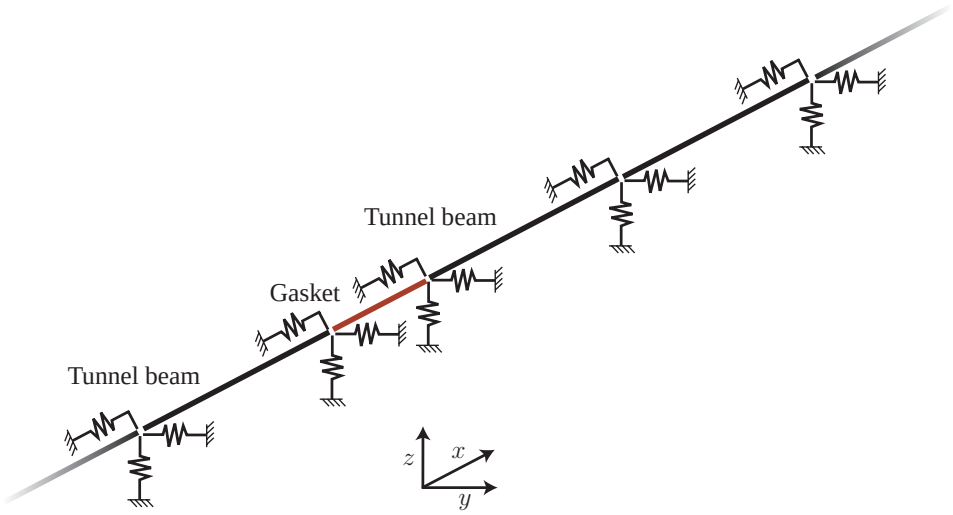

Figure 1: Winkler model of the sectioned tunnel.

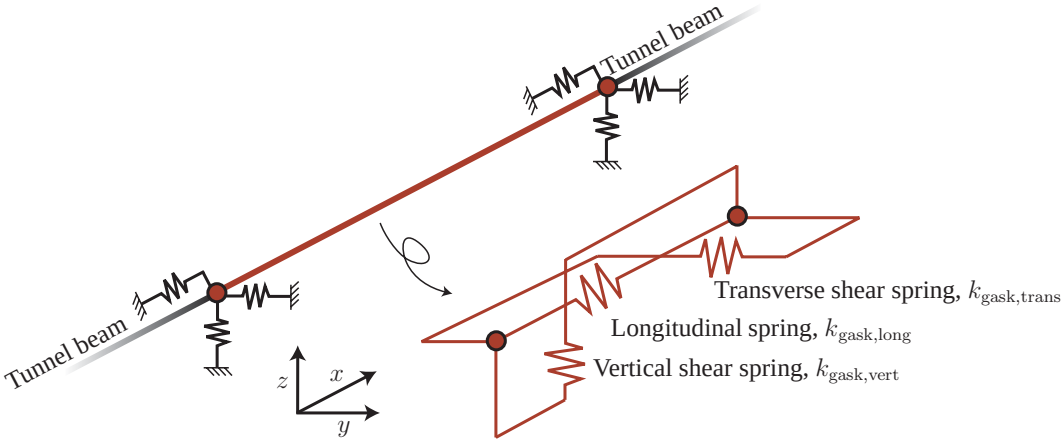

Figure 2: Detailed illustration of the gasket model.

vertical direction, the transverse direction and the longitudinal direction, i.e. the z, the y and the x-directions. Furthermore, the springs act locally, i.e. there is no communication of the response along the tunnel via the soil [9]. Consequently, for the sectioned tunnel considered in the present study, adjacent tunnel elements only interact via the gaskets, modelled by three translational springs, cf. Fig. 2. The validity of this assumption is discussed in Section 4.

2.1 Earthquake motion at bedrock

An acceleration time series from the $M_s = 6.2$ Aegion 1995 earthquake event forms the basis of the present study. This time series has been chosen due to the geographical proximity of Thessaloniki and Aegion, see Fig. 3. The horizontal accelerations sampled at a rate of 100 Hz in an outcropping bedrock are plotted in Fig. 4. The amplitude spectrum is obtained by Fourier transformation of the displacement time series found after integration of the acceleration time series twice with respect to time and corrected to ensure zero displacements at the end of the earthquake. To obtain a smooth

Figure 3: Location of Thessaloniki and Aegion.

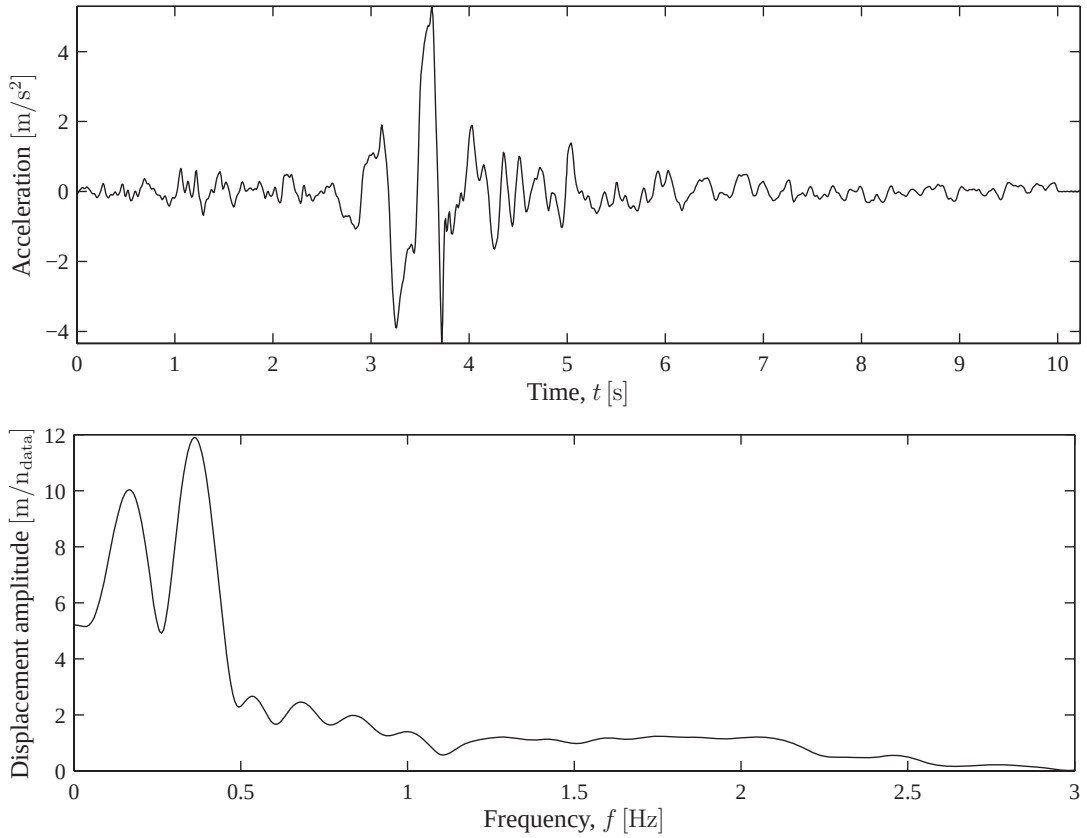

Figure 4: The Aegion 1995 event: Measured horizontal acceleration time series (top); single-sided horizontal displacement amplitude spectrum (bottom).

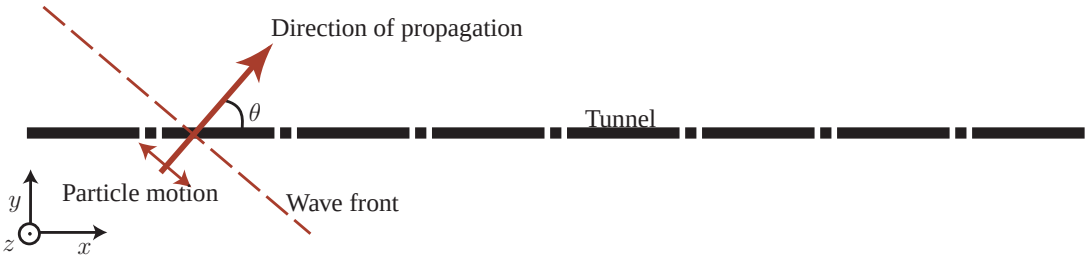

Figure 5: Definition of the propagation direction angle θ.

spectrum and a periodic signal, the time series has been padded with additional zeroes, thus yielding a higher resolution of the Fourier transformation.

The incoherence of the ground motion is significant for the damage imposed on the tunnel. In the present study, the incoherence is described by means of an apparent propagation velocity, c_a, providing the propagation speed of the wavefront measured along the surface of the ground [10]. Here, the apparent velocity $c_a = 1500\ \mathrm{m/s}$ has been chosen in accordance with [4]. Further, it is assumed that the waves propagate in the direction forming the angle $\theta = 45^\circ$ with the tunnel axis in the horizontal plane, cf. Fig. 5. It has been found that this angle of incidence provides the critical combination of compression/extension and longitudinal bending of the tunnel [11].

2.2 Wave transmission through layered soil

As illustrated in Fig. 6, the ground is simplified as a horizontally layered stratum, each layer being modelled as an isotropic linear elastic material. Further, only the horizontally polarized shear waves generated by the forced displacements at bedrock are considered. Hence, the shear wave propagation in a given layer, marked by the superscript j, is governed by the one-dimensional wave equation

$$\frac{\partial^2 u^j(z^j,t)}{\partial z^2} = \frac{1}{(c_S^j)^2}\frac{\partial^2 u^j(z^j,t)}{\partial t^2}, \qquad c_S^j = \sqrt{\frac{\mu^j}{\rho^j}}, \tag{1}$$

where $u^j(z^j,t)$ is the displacement in the horizontal direction orthogonal to the direction of propagation, measured at the local depth z^j within the jth layer. Further, ρ^j and μ^j are the mass density and the shear modulus, respectively, and c_S^j is the corresponding phase velocity of shear waves propagating within the layer.

A frequency-domain solution is established by Fourier transformation of Eq. (1). After discretization, the displacement is represented by a complex Fourier series with N equally spaced discrete frequencies, ω_n, i.e.

$$u^j(z^j,t) \approx \sum_{n=1}^{N} U_n^j(z^j)\mathrm{e}^{\mathrm{i}\omega_n t}, \tag{2}$$

where $\mathrm{i} = \sqrt{-1}$. Each complex amplitude function, $U_n^j(z^j)$, must satisfy the equation

$$\frac{\partial^2 U_n^j(z^j)}{\partial z^2} = -(k_n^j)^2 U_n^j(z^j), \qquad k_n^j = \frac{\omega_n}{c_S^j}, \tag{3}$$

where k_n^j is identified as a wavenumber, and the general solution takes the form:

$$U_n^j(z^j) = B_n^j \mathrm{e}^{\mathrm{i}k_n^j z^j} + C_n^j \mathrm{e}^{-\mathrm{i}k_n^j (z^j - h^j)}. \tag{4}$$

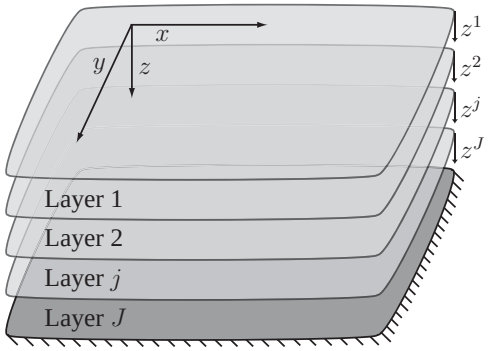

Figure 6: Horizontally stratified soil with definition of local z-axes. The planes illustrate the interfaces separating the soil layers.

The coefficients B^j and C^j depend on the boundary conditions at the top and bottom of the layer, and h^j is the layer depth. Accordingly, the horizontally polarised shear stress within the jth layer becomes

$$P_n^j(z^j) = \mathrm{i}k_n^j\mu^j \left(B_n^j \mathrm{e}^{\mathrm{i}k_n^j z^j} - C_n^j \mathrm{e}^{\mathrm{i}k_n^j (z^j - h^j)} \right). \tag{5}$$

The expressions for $U_n^j(z^j)$ and $P_n^j(z^j)$ may conveniently be combined into

$$\mathbf{S}_n^j(z^j) = \begin{bmatrix} U_n^j(z^j) \\ P_n^j(z^j) \end{bmatrix} = \mathbf{A}_n^j(z^j) \begin{bmatrix} B_n^j \\ C_n^j \end{bmatrix}, \tag{6}$$

where

$$\mathbf{A}_n^j(z^j) = \begin{bmatrix} \mathrm{e}^{\mathrm{i}k_n^j z^j} & \mathrm{e}^{-\mathrm{i}k_n^j (z^j - h^j)} \\ \mathrm{i}k_n^j \mu^j \mathrm{e}^{\mathrm{i}k_n^j z^j} & -\mathrm{i}k_n^j \mu^j \mathrm{e}^{-\mathrm{i}k_n^j (z^j - h^j)} \end{bmatrix}. \tag{7}$$

Defining $\mathbf{S}_n^{j0} = \mathbf{S}_n^j(0)$ and $\mathbf{S}_n^{j1} = \mathbf{S}_n^j(h^j)$, the deformations and stresses at the top of the jth layer can be computed by introduction of a transfer matrix, $\mathbf{T}_n^{j0}$,

$$\mathbf{S}_n^{j0} = \mathbf{T}_n^{j0} \mathbf{S}_n^{J1}, \qquad \mathbf{T}_n^{j0} = \mathbf{A}_n^{j0} \left\{ \mathbf{A}_n^{j1} \right\}^{-1} \mathbf{A}_n^{j+1,0} \left\{ \mathbf{A}_n^{j+1,1} \right\}^{-1} \cdots \mathbf{A}_n^{J0} \left\{ \mathbf{A}_n^{J1} \right\}^{-1} \tag{8}$$

where $\mathbf{A}_n^{j0} = \mathbf{A}_n^j(0)$ and $\mathbf{A}_n^{j1} = \mathbf{A}_n^j(h^j)$. With $\bar{U}_n$ denoting the amplitude of the forced displacement at bedrock, i.e. at the bottom of layer J, the amplitudes of the displacements and stresses at the interfaces are obtained by

$$\mathbf{S}_n^{j0} = \begin{bmatrix} U_n^{j0} \\ P_n^{j0} \end{bmatrix} = \begin{bmatrix} T_{11}^{j0} & T_{12}^{j0} \\ T_{21}^{j0} & T_{22}^{j0} \end{bmatrix} \begin{bmatrix} \bar{U}_n \\ P_n^{J1} \end{bmatrix}. \tag{9}$$

Assuming that the surface, i.e. the seabed, is free of traction, and disregarding the tunnel, the amplitude P_n^{J1} of the stress at bedrock can be derived:

$$0 = \bar{U}_n T_{21}^{10} + P_n^{J1} T_{22}^{10} \qquad \Rightarrow \qquad P_n^{J1} = -\frac{\bar{U}_n T_{21}^{10}}{T_{22}^{10}}. \tag{10}$$

Hence, the deformation at the top of the jth layer can be expressed explicitly as

$$U_n^{j0} = \left(T_{11}^{j0} - \frac{T_{12}^{j0} T_{21}^{10}}{T_{22}^{10}} \right) \bar{U}_n = H_n^{j0} \bar{U}_n, \qquad H_n^{j0} = T_{11}^{j0} - \frac{T_{12}^{j0} T_{21}^{10}}{T_{22}^{10}}. \tag{11}$$

In the frequency domain, hysteretic material damping is introduced by the loss factor η^j, resulting in a complex shear modulus,

$$\mu^j = \left(1 + \mathrm{i}\,\mathrm{sign}(\omega)\eta^j\right) \frac{E^j}{2(1+\nu^j)}, \tag{12}$$

where E^j and ν^j are the real Young's modulus and Poisson's ratio, respectively. According to Eqs. (1) and (13), this provides a complex phase velocity and wavenumber.

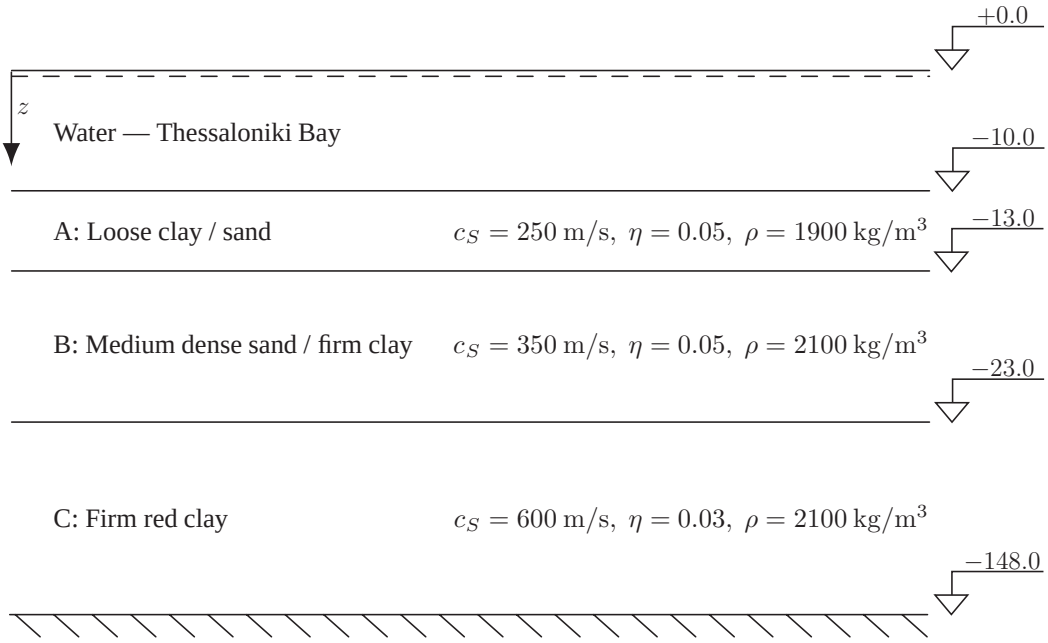

Figure 7: Stratification of the subsoil at Thessaloniki. Depths are given in metres.

Material properties for the Thessaloniki site are listed in Fig. 7, where the real phase velocities and loss factors are determined based upon [12], finding the loss factors as the reciprocal value of the expectation value of the corresponding quality factors, cf. [10]. The mass densities have been estimated, and the phase velocities should be adjusted to account for material damping in accordance with the discussion above.

Based on the method outlined in this section, the response at the ground surface and the tunnel base have been determined for the Aegion event, cf. Fig. 4. The amplitude spectra and the displacement time series are plotted in Figs. 8 and 9, respectively. A significant amplification of the bedrock motion is observed at the resonance frequency $f_1 = 1.09$ Hz, and strong ground vibration continues for about 30–60 s after the passage of the earthquake.

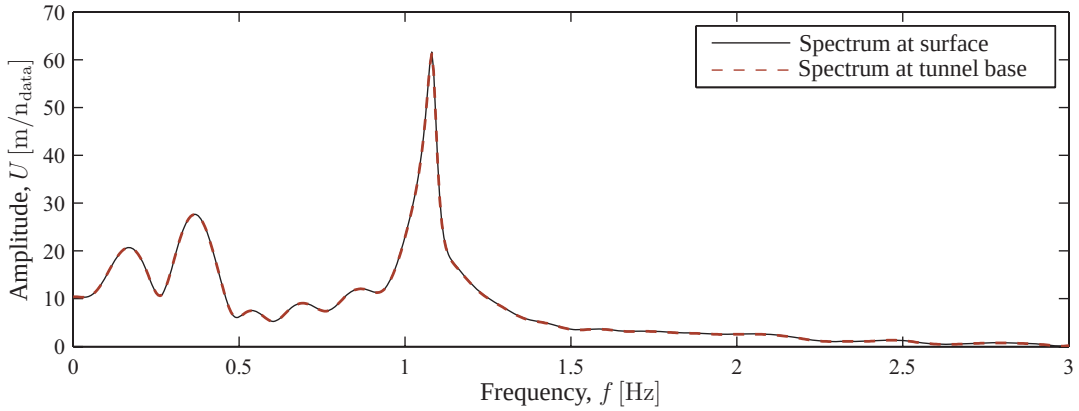

Figure 8: Response spectra at the surface as well as the tunnel base.

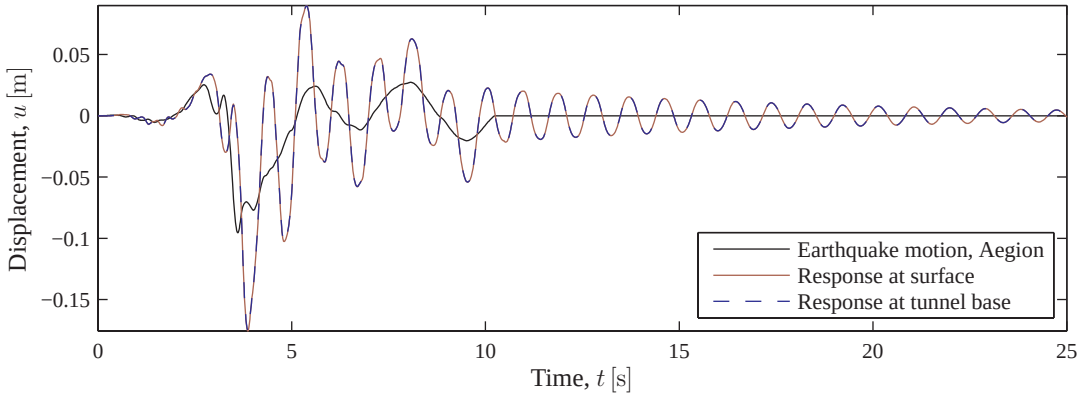

Figure 9: Bed rock motion and response at the surface as well as the tunnel base.

2.3 Calibration of the Winkler model

The eight tunnel elements are modelled by Bernoulli-Euler beam finite elements. A convergency study shows that 20 elements per tunnel element ensures an adequate accuracy of the solution. The cross-sectional area is $A = 111.6\ \mathrm{m}^2$ and the second moments of area about the y- and z-axes are $I_{yy} = 1315\ \mathrm{m}^4$ and $I_{zz} = 12\,650\ \mathrm{m}^4$, respectively. These properties are based on the geometry illustrated in Fig. 10, where it is noted that the cross section is double symmetric. The tunnel elements are made by reinforced concrete, assuming an isotropic linear viscoelastic material model. The material properties are identical to the properties applied in Section 3.

The gasket stiffness is assumed to be linear, which is a crude approximation, since the gasket stiffness increases significantly with the contact pressure between the tunnel elements. Furthermore, shear keys are typically installed in order to prevent strong relative transverse and vertical motion between adjacent elements. The total length of the gasket is 84.4 m (see Fig.10) and the stiffness is assumed to be $24 \cdot 10^6\ \mathrm{N/m/m}$. This corresponds the tangent stiffness of a Gina gasket [13] measured at the Busan-Geoje Fixed Link [14] for a contact pressure of $48{\cdot}10^6\ \mathrm{N/m^2}$ arising due to hydrostatic pressure on the sealed tunnel ends during installation at 16 m water depth. With

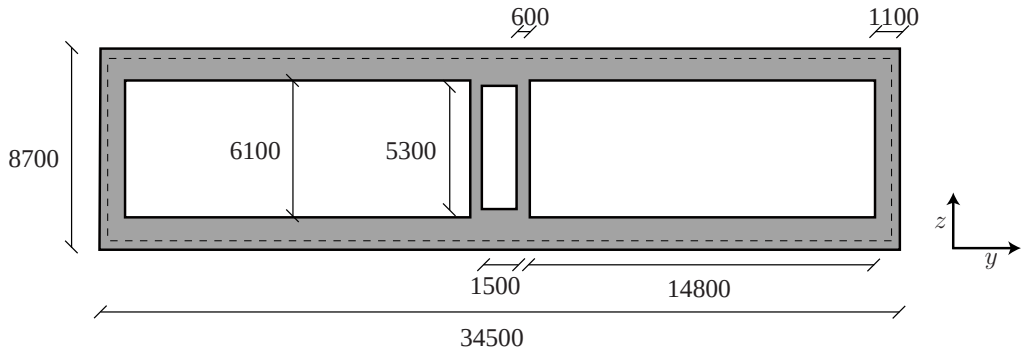

Figure 10: Assumed cross section of the tunnel at Thessaloniki. The dotted line around the perimeter shows the location of the gasket. All measures in mm.

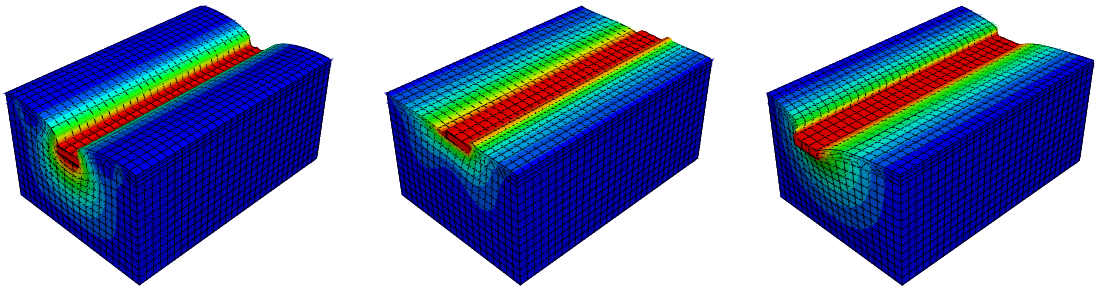

Figure 11: Deformation of the finite-element model utilised for calibration of subgrade spring stiffnesses in the Winkler model: Vertical displacement (left); transverse displacement (middle); longitudinal displacement (right). The colour shades (from blue over green to red) indicate the relative magnitudes of the displacement.

reference to Fig. 2, the three spring stiffnesses are $k_{\mathrm{gask,long}} = 2.05 \cdot 10^9 \ \mathrm{N/m}$ and $k_{\mathrm{gask,vert}} = k_{\mathrm{gask,trans}} = 0.68 \cdot 10^9 \ \mathrm{N/m}$. It has been assumed that the shear modulus is one-third of Young's modulus, corresponding to an isotropic incompressible material.

The spring stiffnesses of the Winkler foundation are calibrated by means of a three-dimensional finite-element (FE) model in ABAQUS [15]. A single tunnel element is considered, represented by a rigid body with a depth of 8.7 mm, a width of 34.5 mm and a length of 153 m. The surrounding soil is modelled by continuum elements using quadratic interpolation of the displacements and reduced integration. The artificial boundaries forming the vertical sides of the model are placed approximately 100 m away from the tunnel, employing the same mesh and geometry as utilised in the full dynamic finite-element analysis described in the next section. The soil is fixed vertically and horizontally at the base as well as the sides. In the computation of the vertical and transverse stiffnesses, the ends of the model are fixed in the x-direction parallel to the tunnel axis. However, for the determination of the longitudinal stiffness, only displacements in the x-direction are allowed at the ends.

Figure 11 shows the deformations due to a load applied to the rigid tunnel element in each of the three directions. The vertical, transverse and longitudinal spring stiffnesses per unit length along the tunnel become $2.668 \cdot 10^9 \ \mathrm{N/m^2}$, $1.492 \cdot 10^9 \ \mathrm{N/m^2}$ and $0.746 \cdot 10^9 \ \mathrm{N/m^2}$, respectively. Alternatively, the vertical and transverse spring stiffnesses may be found by a two-dimensional analysis, since plane strain can be assumed. A computation carried out by PLAXIS [16], using a finer mesh and 15-noded triangular elements with fourth-order spatial interpolation, indicates that the error on the stiffnesses determined by the three-dimensional FE model is below 2%.

3 Continuum finite-element model of tunnel and soil

A three-dimensional finite-element analysis (FEA) is carried out in ABAQUS, again assuming linear response of the soil, tunnel and gasket materials. Whereas the hysteretic material damping model is suitable for soil, it is inconvenient in the present case, since a direct solution in time domain is not possible. Hence, an equivalent lin-

ear viscous damping model may be applied, providing the same amount of damping at the first resonance frequency of the soil column, f_1, i.e.

$$\mu^j = \left(1 + \mathrm{i}\,\omega\beta^j\right) \frac{E^j}{2(1+\nu^j)}, \qquad \beta^j = \frac{\eta^j}{2\pi f_1}. \tag{13}$$

With reference to Fig. 8 the viscous damping model is calibrated for the frequency $f_1 = 1.09$ Hz. The resulting material properties employed in the three-dimensional FEA are listed in Table 1, where reinforced concrete is used to model the tunnel.

The soil surrounding the tunnel is modelled as a single part, divided into three layers (see Fig. 7) and containing a cavity to accommodate the tunnel, cf. Fig. 12. Each tunnel element is modelled as a separate part with the length 153 m and the cross section defined in Fig. 10. A meshed tunnel element is illustrated in Fig. 13. Finally, the gaskets are modelled by continuum elements, employing an orthotropic

Table 1: Material data for the ABAQUS model.

Material	Density ρ [kg/m^3]	Young's modulus E [Pa]	Poisson's ratio ν [-]	Damping β [-]
Soil layer A	1900	$0.35 \cdot 10^9$	0.49	$7.30 \cdot 10^{-3}$
Soil layer B	2100	$0.76 \cdot 10^9$	0.48	$7.30 \cdot 10^{-3}$
Soil layer C	2100	$2.19 \cdot 10^9$	0.45	$4.38 \cdot 10^{-3}$
Reinforced concrete	2500	$40 \cdot 10^9$	0.15	$1.46 \cdot 10^{-3}$

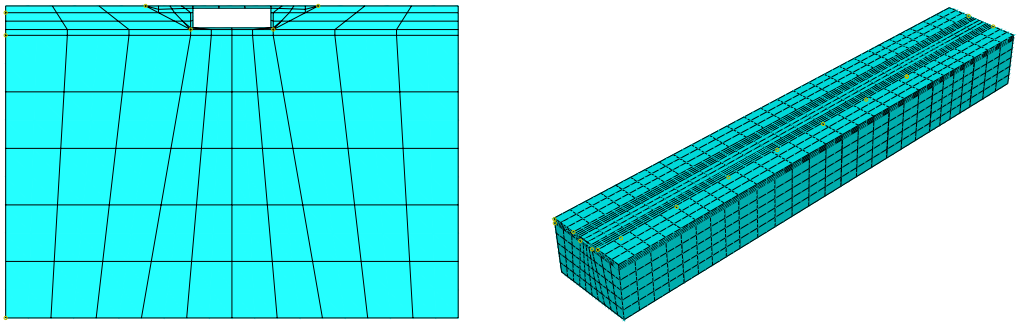

Figure 12: The meshed subsoil: Cross section (left); isometric view (right).

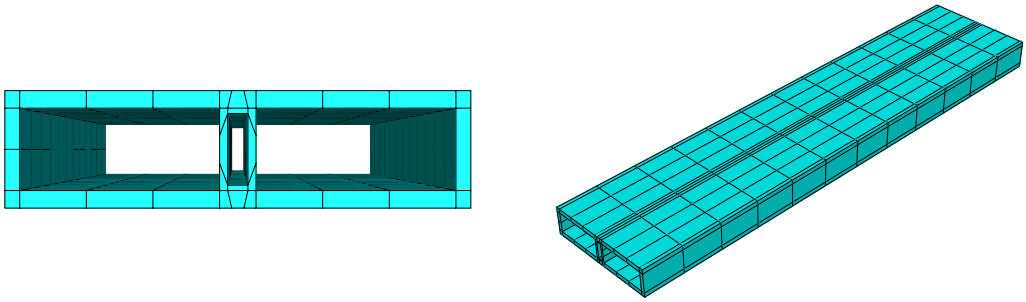

Figure 13: The meshed tunnel element: Cross section (left); isometric view (right).

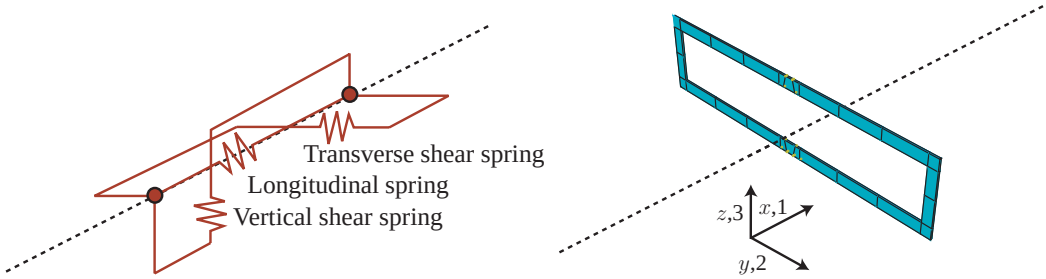

Figure 14: Gasket modelling in the Winkler model (left) and continuum model (right).

linear material model. The gasket is 0.2 m thick and covers the entire solid cross section of the tunnel. Hence, a model equivalent to the longitudinal springs in the Winkler approach is achieved with a Young's modulus of $E_1 = 3.98 \cdot 10^6\ \mathrm{N/m^2}$ in the x-direction, i.e. along the tunnel as shown in Fig. 14. The shear moduli $G_{12} = G_{13} = G_{23} = E_1/3$ are applied, and the Poisson's ratios are defined as $\nu_{12} = \nu_{13} = \nu_{23} = 0$ in order to avoid interaction between the stresses and deformations in the longitudinal, transverse and vertical directions. This mimics the behaviour of the Winkler model.

It is noted that the values of E_2 and E_3 for the gasket are unimportant, since the outer faces of the gaskets are uncoupled from the soil. For all other interfaces, the soil–structure interaction is modelled by surface-to-surface ties in the assembly of the multiple parts. Hence, the remaining interfaces in the model are all assumed to be rough, disallowing slip and sliding between the soil and the structure. This may not be realistic, but corresponds to the assumptions made in the Winkler model.

Quadratic spatial interpolation with reduced integration is employed, using brick and wedge elements with 20 and 15 nodes, respectively [15]. The longest side of an element in the FE model is about 38.5 m, corresponding to a minimum of 7 elements per wavelength for frequencies below 2 Hz. The constant time step $\Delta t = 0.01\ \mathrm{s}$ has been used, providing a Courant number well below 1.0 in most parts of the model; but the finite elements used for the tunnel are stiff and thin, resulting in a Courant number much higher than one. However, computations carried out with time steps of 0.001 s and 0.005 s show that the accuracy of the model is only slightly affected.

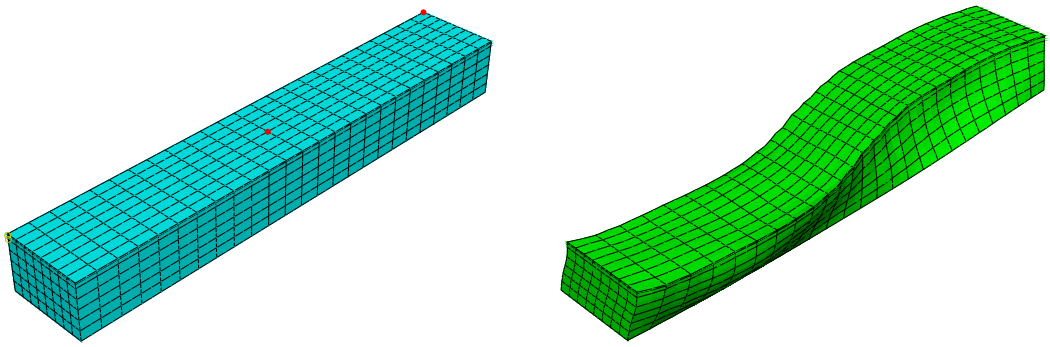

Figure 15: Soil domain used for validation of the FE model: Definition of observation nodes (left); deformation at $t = 6\ \mathrm{s}$ with $c_a = 1500\ \mathrm{m/s}$ and $\theta = 0^\circ$ (right).

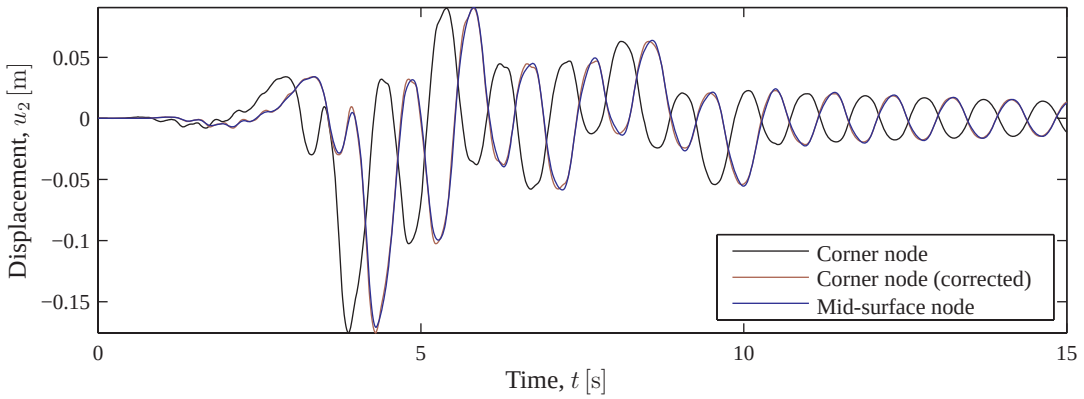

Figure 16: Displacement time series for the two observation nodes. The red line is the corner node displacement corrected for the time shift caused by the apparent velocity.

The surface of the ground is free of traction. On the remaining part of the boundary, displacements are prescribed. The displacements at the bedrock are determined directly from the recorded time series, using the apparent velocity c_a and the wave propagation angle θ to define the spatial and temporal incoherence of the motion. The displacements on the vertical boundaries, i.e. the sides and ends of the modelled soil domain, are determined from the bedrock motion utilising the method outlined in Subsection 2.2. Hence, it is assumed that the ground motion in the far field is independent of the tunnel, and furthermore the wave propagation can be analysed as one-dimensional—except for the apparent velocity. To check the validity of this approach, a model has been created as illustrated in Fig. 15. The transverse displacement time series at the two observation nodes highlighted in the figure are plotted in Fig. 16. It is noted that hysteretic damping has been assumed in the frequency-domain solution employed for the evaluation of the forced displacements at the boundary, whereas linear viscous damping is present in the FE model. This may be responsible for the entire deviation between the results obtained at the corner node and the mid-surface node. Hence, the assumption of one-dimensional wave propagation is valid.

4 Results and discussion

In this section, the models outlined in Sections 2 and 3 will be applied for the analysis of the Thessaloniki tunnel subjected to the Aegion 1995 event. The focus of the discussion is the accuracy of the Winkler method in assessing the damage on the sectioned tunnel. For this reason, a damage criterion has to be defined.

Generally, tunnels subjected to seismic loading can fail due to a number of reasons, including axial deformation by compression and extension of the tunnel structure, hoop deformation (ovalisation) of the tunnel cross section, curvature deformation by longitudinal bending of the tunnel structure, racking of the tunnel cross section [17]. However, in the case of a sectioned tunnel with concrete tunnel elements separated by

Gina gaskets, it is expected that deformations are localised at the joints, i.e. relative displacements and rotations occur between adjacent tunnel elements [6]. This is critical, since a loss of the contact pressure and, as a consequence of this, a loss of the watertightness arises in a gasket.

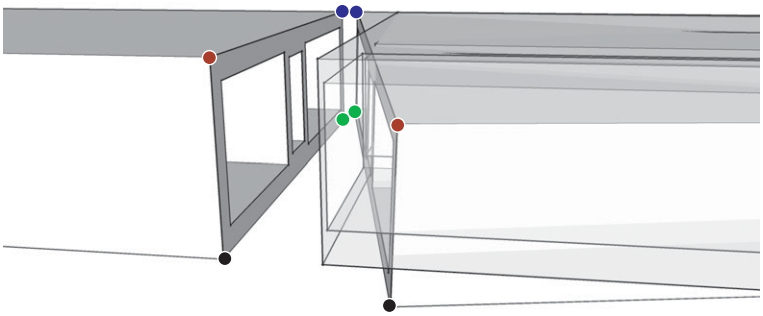

Figure 17: Sketch of two tunnel element ends. For the right tunnel element, the deformed and undeformed (transparent) states are shown, with a considerable (exaggerated) relative displacement and rotation. The Gina gasket is not shown. The colours indicate which corners that are related when calculating the gasket damage.

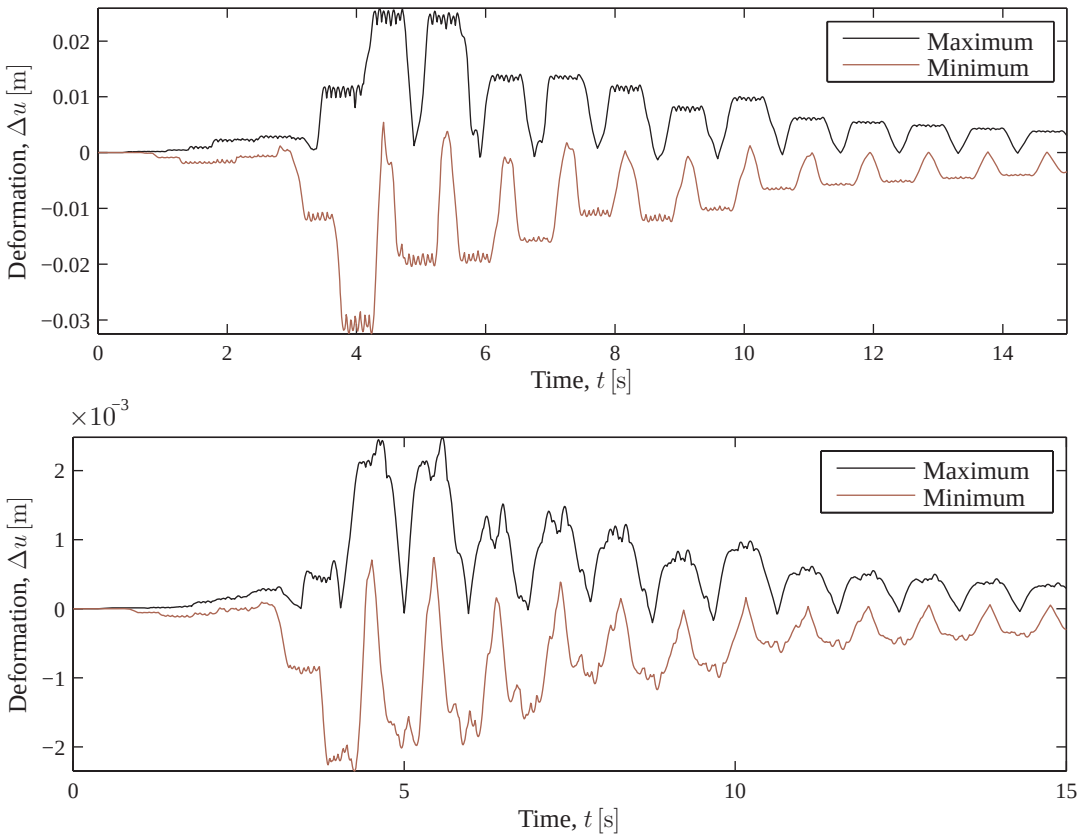

Figure 18: Boundaries for the relative gasket corner deformations: Winkler model (top); continuum model (bottom).

Hence, in the present analysis, the damage criterion is based on the relative motion of the tunnel cross sections at the ends of two neighbouring tunnel elements. The maximum gap will appear a one of the corners, given that the tunnel cross section remains plane during deformation. This is one of the basic assumptions of the Bernoulli-Euler beam theory applied in the Winkler model and will as well be assumed in the assessment of the results from the three-dimensional continuum finite-element analysis (FEA). Hence, the relative displacements between the nodes highlighted in Fig. 17 will be used for the evaluation of damage.

The displacement time series corresponding to the Aegion 1995 event has been used as input at bedrock. In accordance with Subsection 2.1, the apparent velocity is $c_a = 1500\ \mathrm{m/s}$ and the propagation angle is $\theta = 45°$. Thus, the maximum openings and overclosures do not occur simultaneously at the corners of different gaskets.

Figure 18 shows the maximum and minimum deformation occurring at any of the 4×7 gasket corners. In the Winkler model, the response at the different gaskets during the passage of the earthquake are nearly identical. Thus, seven small tips and dips are identified in the response for each major cycle. This is less pronounce in the FEA, but qualitatively the results of the Winkler model and the FEA look similar. However, quantitatively the Winkler model provides relative deformations at the gaskets that are

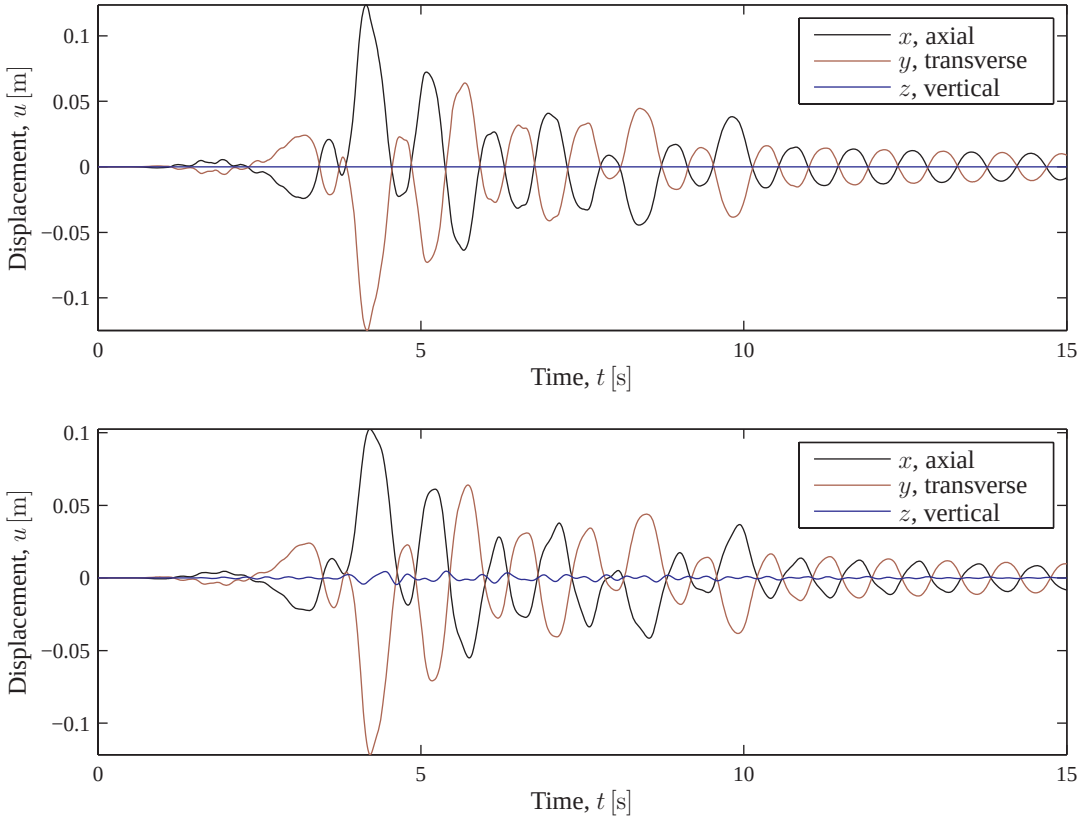

Figure 19: Displacements at a gasket corner: Winkler model (top); continuum model (bottom).

one order of magnitude higher than the results of the ABAQUS model. Given that the continuum model of the soil is more accurate than the disjoint spring approach, the Winkler model provides a overly conservative result regarding the damage risk. Additional analyses show that the relative displacements obtained by the Winkler model in the present case are only slightly more accurate than the results obtained by a simple closed-form solution based on free-field conditions [18] and lumping all axial deformations at the gaskets [11].

The reason to the discrepancy between the results of the Winkler model and the continuum model is discussed in the following. Firstly, the displacements at one of the top corners of the midmost gasket are analysed to check whether the response is similar in the two models. As shown in Fig. 19, a maximum absolute displacement of approximately 0.12 m in the x-direction is predicted by the Winkler model, which is about 20% more than the similar displacement obtained by the continuum model. Further studies indicate that the displacements obtained by the two methods at all individual corner nodes are of the same magnitude. A similar analysis has been carried out for a tunnel without gaskets, i.e. with a homogeneous concrete cross section [11]. Here, the difference between the responses obtained by the Winkler model and the three-dimensional FEA is insignificant. Thus, the Winkler model provides an accurate estimation of the response of uniform extended underground structures.

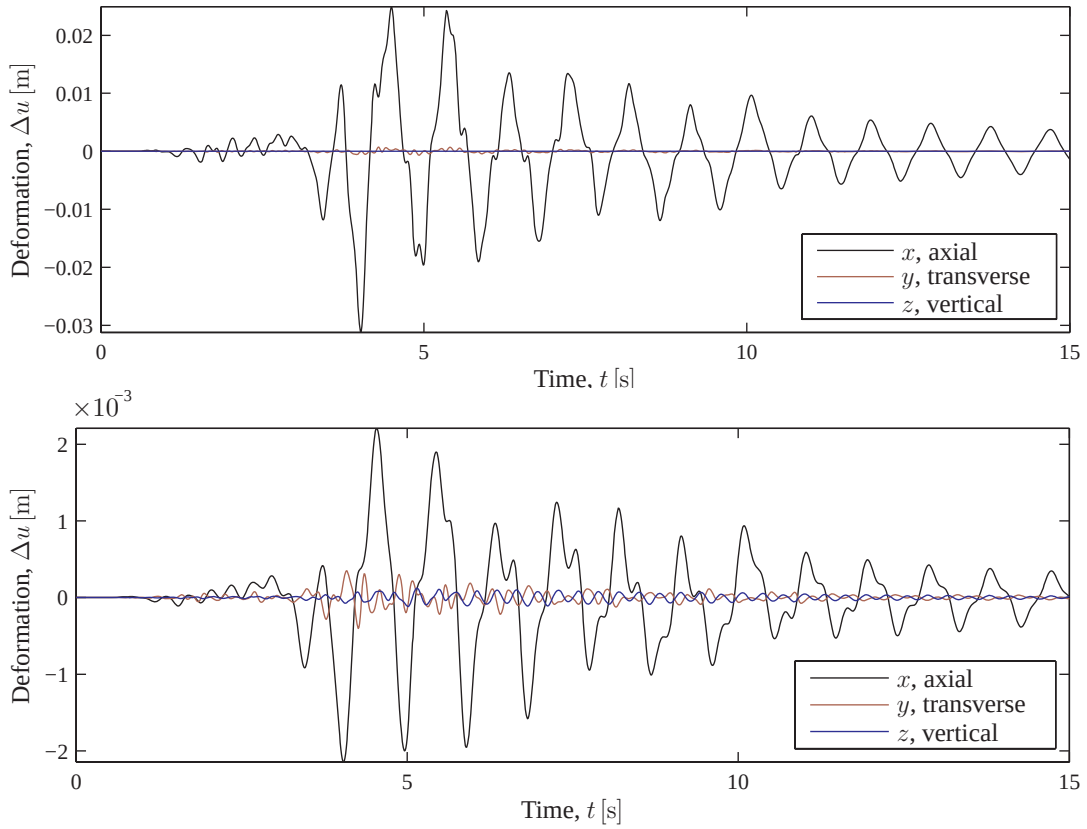

Figure 20: Relative translational deformation of the midmost gasket centre: Winkler model (top); continuum model (bottom).

A comparison of Figs. 18 and 19 shows that the total displacements are one order of magnitude greater than the relative displacements at a gasket in the Winkler model and two orders of magnitude greater in the continuum model. Thus, with similar total displacements at the tunnel ends, the relative deformation across a gasket is ten times greater in the Winkler model than obtained in the continuum model, suggesting that a better model of the gasket is necessary in the Winkler model.

With reference to Fig. 2, the gasket is modelled as three uncoupled translational springs in the Winkler model. Whether the inclusion of rotational springs is required has been examined by analysis of the relative contributions to the opening and compression at a gasket corner from translation and rotation of the tunnel element ends. The results of the analysis regarding the translation are provided in Fig. 20, whereas the results regarding the rotation are given in Fig. 21. Clearly, the contributions to the total relative deformation at a gasket corner from the longitudinal translation of the tunnel cross sections dominate in the Winkler model as well as the continuum model. In particular it is observed that the rotations of the cross section only provide about 10% of the total relative displacement, i.e. the contribution from longitudinal bending is small compared to the contribution from translation of the tunnel elements in the present case. Therefore, inclusion of rotational springs at the joints in the Winkler model will not improve the overall accuracy significantly.

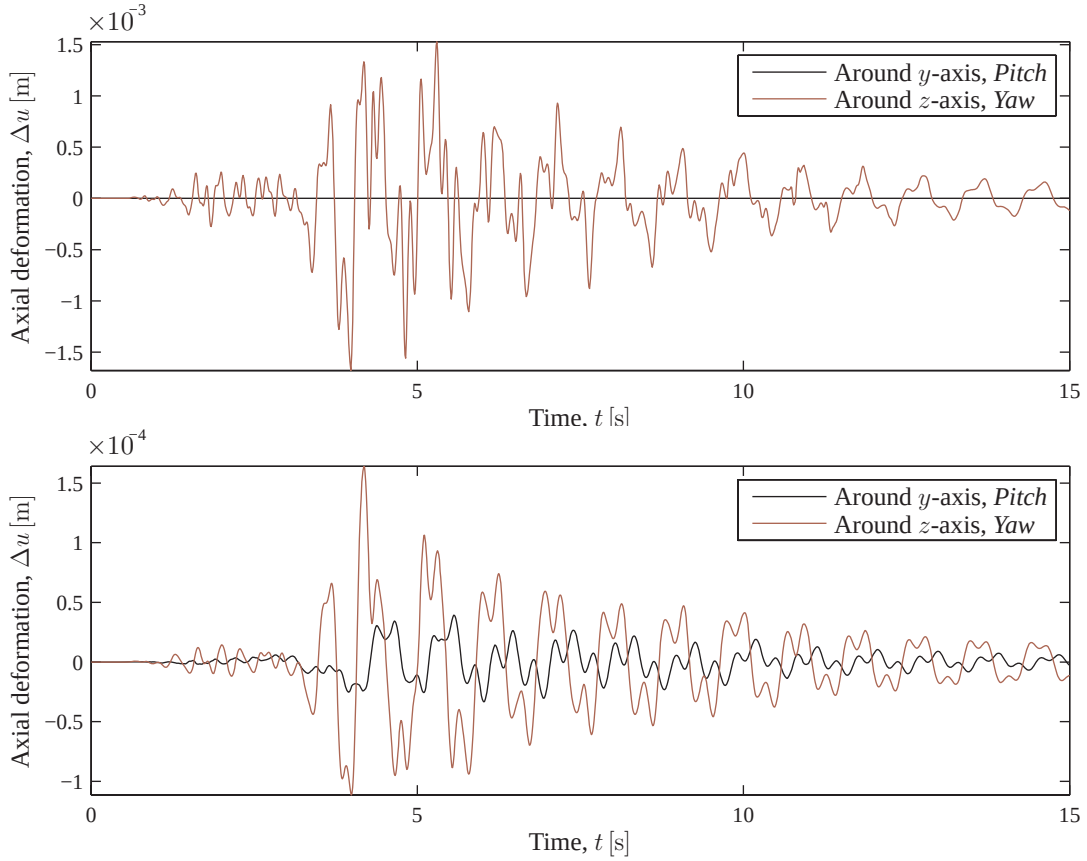

Figure 21: Gasket corner deformation due to rotations of the midmost gasket centre around the y-axis and the z-axis: Winkler model (top); continuum model (bottom).

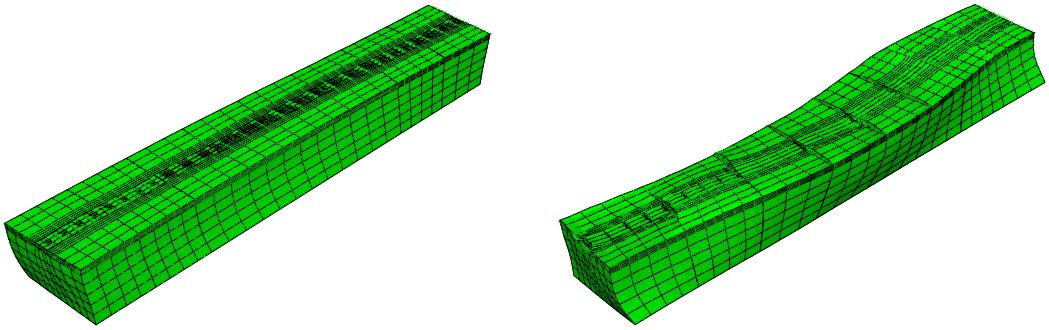

Figure 22: Deformed domain for an analysis *without* separation planes (left) and *with* separation planes (right). The displacements are exaggerated and plotted at different instants of time.

Hence, another explanation must be given for the discrepancy between the results of the Winkler model and the continuum model. Since the tunnel elements in the ABAQUS model almost deform like beams, the major difference is the modelled behaviour of the soil. Thus, no retroaction across the joints via the soil is included in the Winkler model, whereas two tunnel elements interact through the soil in the continuum model. The improvement of the Winkler model to account for retroaction is not straightforward. Instead, the impact of retroaction is tested by comparison of two ABAQUS models, the first of which is the model already discussed. In the second model, the soil at the gasket planes is modelled without stiffness and mass, such that waves will not be transmitted through these "separation planes".

An illustration of the response at a given time step is presented in Fig. 22. Clearly, localised deformations occur around the separation planes. An investigation of the time series of the gasket opening at the seven joints leads to the result that a maximum relative displacement of about 70 mm is obtained. This is about twice the deformation provided by the Winkler model and more than 30 times the deformation achieved without the separation planes in the original ABAQUS model. Thus, the dominating error in the Winkler model of the sectioned tunnel is the lacking ability to account for retroaction via the soil at the tunnel joints. It has been tested by variation of the soil stratification, propagation direction and apparent propagation velocity [11] that the problem identified regarding the Winkler model is consistent for the present tunnel.

5 Conclusion

A Winkler-type model has been applied to the analysis of a sectioned tunnel subject to seismic loading, transferred from bedrock to the tunnel via a stratified soil. By comparison with a three-dimensional continuum finite-element model it has been found that the relative deformations at a joint between two adjacent tunnel elements is overestimated by a factor ten with the Winkler model. Hence, the Winkler model provides a highly conservative design of immersed sections tunnels where the relative displacements at a gasket may cause loss of watertightness. However, for a tunnel

with a uniform cross section, the Winkler model provides result of an adequate accuracy. The great error in the results of the Winkler model are explained by the missing ability to account for retroaction via the soil across a joint. The improvements of the Winkler model, necessary for the design of sectioned tunnels, will be the target of future research.

References

[1] G.P. Kouretzisa, G.D. Bouckovalasa and C.J. Gantesb, "3-D Shell Analysis of Cylindrical Underground Structures Under Seismic Shear (S) Wave Action", Soil Dynamics and Earthquake Engineering, 26(10), 909–921, 2006.

[2] A.A. Stamos and D.E. Beskos, "3-D Seismic Response Analysis of Long Lined Tunnels in Half-space", Soil Dynamics and Earthquake Engineering, 15(2), 111-Ű118, 1996.

[3] K. Haciefendioğlu, and A. Bayraktar, "Stochastic response of underground structures", Proceedings of the Institution of Civil Engineers: Geotechnical Engineering, 161(6), 325–339, 2008.

[4] C. Vrettos, B. Kolias, T. Panagiotakos and T. Richter, "Seismic Response Analysis of an Immersed Tunnel Using Imposed Deformations", in "Proceedings of the 4th International Conference on Earthquake Geotechnical Engineering", paper no. 1473, 2007.

[5] O. Kiyomiya, "Earthquake-resistant Design Features of Immersed Tunnels in Japan", Tunnelling and Underground Space Technology, 10(4), 463–475, 1995.

[6] I. Anastasopoulos, N. Gerolymos, V. Drosos, R. Kourkoulis, T. Georgarakos and G. Gazetas, "Nonlinear Response of Deep Immersed Tunnel to Strong Seismic Shaking" Journal of Geotechnical and Geoenvironmental Engineering, 133, 1067–1090, 2007.

[7] COWI, "http://www.cowi.com/projects/transport", visited: May 13, 2009.

[8] P.B. Schnabel, J. Lysmer and H.B. Seed, "SHAKE–a Computer Program for Earthquake Response Analysis of Horizontally Layered Sites". Report No. EERC 72-12, Berkeley: University of California, 1972.

[9] D.J. Dowrick, "Earthquake Resistant Design: For Engineers and Architects", 2nd edition, John Wiley & Sons, 1987

[10] S.L. Kramer, "Geotechnical Earthquake Engineering", Prentice Hall, 1996.

[11] J.H. Lyngs,"Model Accuracy in Asseismic Design of Immersed Tunnel", Master's Thesis, School of Civil Engineering, Aalborg University, Aalborg, Denmark, 2008.

[12] A. Anastasiadis, D. Raptakis and K. Pitilakis, “Thessaloniki’s Detailed Microzoning: Subsurface Structure as Basis for Site Response Analysis”, Pure and Applied Geophysics, 158, 2597–2633, 2001.

[13] Trelleborg Bakker BV, “http://www.trelleborg.com/bakker”, visited: May 13, 2009.

[14] Daewoo, “Busan-Geoje Fixed Link–Immersed Tunnel, Seismic Analysis and Design”, Daewoo Engineering & Construction CO. Ltd., 2004.

[15] ABAQUS Version 6.8 Documentation, Dassault Systèmes Simulia Corp, Providence, Rhode Island, USA, 2008.

[16] R.B.J. Brinkgreve (edt.), PLAXIS 2D – Version 8 Manual, A.A. Balkema Publishers, Lisse, The Netherlands, 2002.

[17] G.N. Owen and R.E. Scholl, “Earthquake engineering of large underground structures”, Federal Highway Administration and National Science Foundation, Report no. FHWA/RD-80/195, 1981.

[18] Y.M.A. Hashash, J.J. Hook, B. Schmidt and J. I-Chiang Yao, “Seismic Design and Analysis of Underground Structures”, Tunnel and Underground Space Technology, 16, 2001.

ISSN 1901-7278
DCE Technical Memorandum No. 10